optica

Stimulated Raman spectroscopic imaging by microsecond delay-line tuning

Chien-Sheng Liao,[1] Kai-Chih Huang,[1] Weili Hong,[1] Andy J. Chen,[2] Caroline Karanja,[3] Pu Wang,[1] Gregory Eakins,[3] and Ji-Xin Cheng[1,3,4,5,6,*]

[1]Weldon School of Biomedical Engineering, Purdue University, West Lafayette, Indiana 47907, USA
[2]Department of Biological Sciences, Purdue University, West Lafayette, Indiana 47907, USA
[3]Department of Chemistry, Purdue University, West Lafayette, Indiana 47907, USA
[4]Purdue University Center for Cancer Research, Purdue University, West Lafayette, Indiana 47907, USA
[5]Birck Nanotechnology Center, Purdue University, West Lafayette, Indiana 47907, USA
[6]School of Electrical and Computer Engineering, Purdue University, West Lafayette, Indiana 47907, USA
*Corresponding author: jcheng@purdue.edu

Received 10 August 2016; revised 30 September 2016; accepted 17 October 2016 (Doc. ID 273497); published 15 November 2016

Stimulated Raman scattering (SRS) microscopy is an emerging platform for vibrational imaging of living systems. We present microsecond-scale SRS spectroscopic imaging by temporally tuning two spectrally focused pulses through a resonant delay line. Our platform is able to acquire an SRS spectrum in 42 μs and form a spectral image of 40,000 pixels within 3.3 s. Spectroscopic identification of single bacteria and fungi in blood and 4-D imaging (x–y–z–λ) of intracellular organelles in live *C. elegans* are demonstrated. © 2016 Optical Society of America

OCIS codes: (170.5660) Raman spectroscopy; (180.4315) Nonlinear microscopy.

http://dx.doi.org/10.1364/OPTICA.3.001377

Coherent Raman imaging techniques, including coherent anti-Stokes Raman scattering (CARS) and stimulated Raman scattering (SRS), are powerful tools to visualize the spatial distribution of molecules in cells or tissues [1–4]. By coherent excitation of a single molecular vibration, the imaging speed at a narrow spectral window has been improved up to video rate [5,6]. To resolve overlapped Raman bands in biological samples, there has been a great effort in developing spectroscopic coherent Raman imaging technology. Spectral scanning of a narrowband laser pulse and collection of images at a series of Raman shifts has reached the speed of a few seconds per stack [7–11]. In these studies, the limited temporal resolution of each spectroscopic measurement on second scale might distort spectral profiles from highly dynamic organelles in live cells or animals. Multiplex CARS by a broadband excitation pulse and a narrowband probe pulse has been demonstrated to simultaneously excite multiple Raman bands and detect spectrally dispersed vibrational signals [12,13] with a pixel dwell time as short as 3 ms [14]. Recently multiplex [15,16] and frequency-multiplexing [17,18] SRS have further reached microsecond spectral acquisition and enabled real-time spectroscopic imaging [15,17].

One simple and efficient way to utilize femtosecond pulses for spectroscopic measurement is to linearly chirp the pump and Stokes pulses and focus their entire bandwidth into a narrow spectral region [19]. In this way, each temporal delay between the chirped pulses corresponds to a Raman shift (Fig. 1(a)). By scanning the temporal delay of one of the pulses and recording a series of images, SRS spectroscopic imaging based on this spectral focusing scheme has been demonstrated with a total acquisition time of several tens of seconds [20,21], where the spectral acquisition speed was limited by the waiting time for stabilization and communication of a motorized translational stage used for delay tuning.

In this work, we overcome the abovementioned limitation and demonstrate SRS spectroscopic imaging using a laboratory-built microsecond delay-line tuner (Fig. 1(b)). By directing the collimated light to the edge of a tilted resonant mirror with a few kilohertz central frequency, and focusing the reflected light with a lens on a flat mirror, the retroreflected light experiences a millimeter-scale difference in optical path when the resonant mirror is scanned in one cycle of tens of microseconds. This method was first demonstrated for optical coherence tomography [22] and more recently applied to Fourier transform CARS spectroscopy [23]. Here we implement a 12 kHz resonant mirror to scan the temporal delay between two chirped pulses for SRS spectroscopic imaging. By synchronization of the resonant mirror with galvo-mirrors used for the imaging scan, we collected an SRS spectrum that covered ~200 cm^{-1} as determined by the excitation pulse, with pixel acquisition time of 83 μs. Our scheme improved the temporal resolution of SRS spectra from seconds to microseconds compared to previous frame-by-frame methods utilizing a motorized stage [20,21]. Because of the spectral acquisition speed on the microsecond scale, we successfully acquired chemical images from highly dynamic organelles in live cells and *C. elegans*.

Our setup is depicted in Fig. 1(b). In brief, a tunable 80 MHz pulsed laser (InSight, Spectra Physics) provided two synchronized outputs. The fixed 1040 nm beam with ~220 fs pulse width as

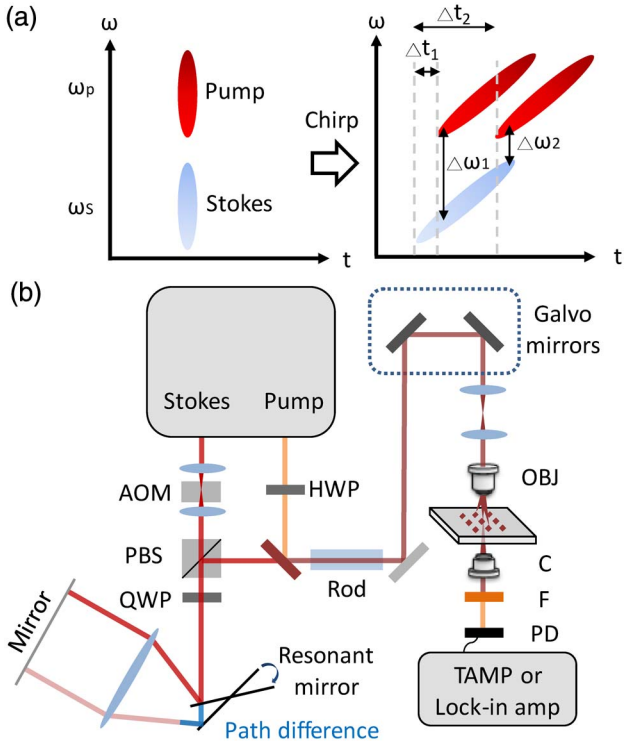

Fig. 1. Concept and setup of SRS spectroscopic imaging by microsecond delay-line tuning. (a) Each temporal delay between the chirped pump and Stokes corresponds to a molecular vibrational mode. (b) Setup. AOM, acousto-optic modulator; C, condenser; F, filter; HWP, half-wave plate; OBJ, objective; PBS, polarizing beam splitter; PD, photodiode; QWP, quarter-wave plate; TAMP, tuned amplifier.

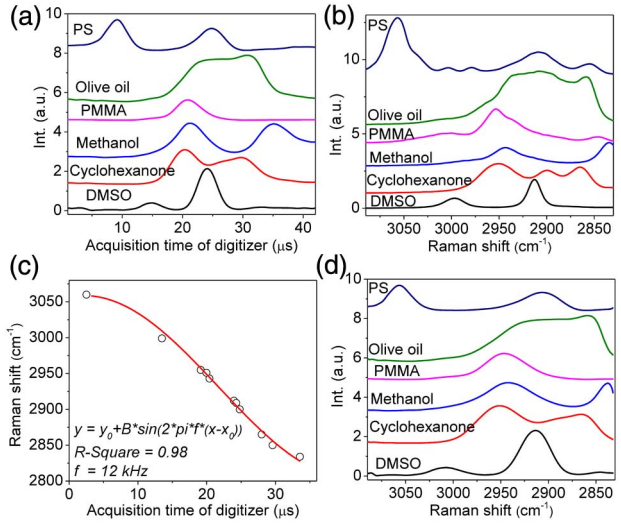

Fig. 2. Spectral calibration. (a) Raw spectra of polystyrene (PS), olive oil, PMMA, methanol, cyclohexanone, and DMSO measured by our setup. (b) Measured by spontaneous Raman spectroscopy. (c) Mapping of Raman shifts to acquisition time of our digitizer with a sinusoidal fitting. (d) Calibrated spectra of (a).

the Stokes beam was first intensity modulated by an acousto-optic modulator at 6.2 MHz, and then directed to the edge of a resonant mirror (CRS 12 kHz, Cambridge). Here, we utilized only the forward movement of the resonant mirror for spectral acquisition. Therefore, the spectral acquisition time for each pixel is 42 μs, and the pixel dwell time is 83 μs. The pulses were focused by an achromatic lens of 100 mm focal length and then reflected by a flat mirror back to the same path. A quarter-wave plate and a polarizing beam splitter together retrieved the retroreflected pulses. For the pump beam, the tunable output from the laser provided a tuning range from 680 to 1300 nm. The pump pulse of ~120 fs pulse width was rotated by a half-wave plate in order to match the polarization of the Stokes beam. Then the pump and Stokes pulses were combined and chirped by two 12.7 cm SF57 rods. The pulse widths of the pump and Stokes beams were stretched to 1.3 ps and 0.8 ps, respectively, measured with an autocorrelator (PulseScope, APE). The combined pulses were then sent to a home-built laser scanning microscope. A 40 × or 60 × objective (LUMPLFLN 40XW, UPLSAPO 60XW, Olympus) focused the pulses on the sample. The maximum optical powers on the sample were 12 mW for 800 nm and 180 mW for 1040 nm. For biological samples, the optical powers were 12 mW for 800 nm and 80 mW for 1040 nm. The SRS signals were collected, filtered, and detected by a photodiode (S3994, Hamamatsu) incorporated with a home-built resonant circuit. The central frequency of the resonant circuit was 6.2 MHz with a 700 kHz bandwidth (see Supplement 1, Fig. S1). The output signals from the resonant circuit were sent to a rectifier reported in our previous work [24] with a bandwidth of 707 kHz or a digital lock-in amplifier with a bandwidth of 203 kHz (HF2LI, Zurich Instrument). The output data was recorded at 5 MHz sampling rate with a digitizer (ATS 460, AlazarTech).

To calibrate the Raman shift and compensate the nonlinearity of the resonant mirror, we compared the spectral profiles acquired with our SRS spectroscopic setup [Fig. 2(a)] to spontaneous Raman spectroscopy [Fig. 2(b)]. Eleven known Raman peaks from six chemicals were used to construct the calibration curve that was fitted with a sinusoidal function [Fig. 2(c)]. The fitted frequency was 12 kHz, which matched the resonant frequency of our scanning mirror. Then the acquisition time of the digitizer was converted into Raman shift [Fig. 2(d)]. We found a spectral coverage of ~200 cm^{-1} corresponding to 3 ps in the optical delay line, confirmed by a motorized translational stage [Fig. 2(d)]. We further characterized the spectral resolution by the known Raman peak of dimethyl sulfoxide (DMSO) solution at 2912 cm^{-1}. By a commercial digital lock-in amplifier with a bandwidth of 203 kHz, 32 cm^{-1} spectral resolution was achieved, and it can be further improved to 25 cm^{-1} by our home-built rectifier with a bandwidth of 707 kHz (see Supplement 1, Fig. S2). The 25 cm^{-1} spectral resolution was consistent with our previous work on SRS spectroscopic imaging using a motorized translational stage for delay-line tuning [21], indicating that the response time of our home-built rectifier circuit is sufficient for the microsecond delay-line scanning.

Compared to the femtosecond pulse-shaping techniques used in our previous works for microsecond SRS spectroscopic imaging [15,17], the main advantage of using spectrally focused femtosecond pulses is the utilization of the full spectral bandwidth in ultrashort pulses. This advantage also leads to better detection sensitivity. To quantify the sensitivity, we acquired SRS spectra from DMSO solutions diluted with D_2O (see Supplement 1, Fig. S3). D_2O exhibited a background contributed by cross-phase modulation, while DMSO showed a distinct Raman peak at 2912 cm^{-1}. Under a pixel dwell time of 83 μs, we detected

0.15% DMSO solution (21.2 mM) with a signal-to-noise ratio of 2.7. This detection sensitivity is 3.3 times better than our previous work under the same integration time [15,17], which can be attributed to the higher remaining laser power (~330 mW) after the optical setup for microsecond delay-line tuning.

To demonstrate the real-time spectroscopic imaging platform enabled by microsecond delay-line tuning, we scanned a sample of mixed microspheres of polystyrene and poly(methyl methacrylate) (PMMA), and acquired 160,000 spectra pixel-by-pixel (see Supplement 1, Fig. S4). The reconstructed SRS image at 2916 cm^{-1} showed the morphology of the mixture. The spectroscopic image data was denoised [25] and decomposed by multivariate curve resolution (MCR) analysis [10] with previously reported algorithms. The MCR output concentration maps of polystyrene and PMMA indicated their spatial distributions, and the output spectra matched the spontaneous Raman data shown in Fig. 2(b).

Our imaging platform is able to resolve chemical compositions of highly dynamic living cells. This advantage enabled rapid detection and analysis of pathogenic microorganisms, i.e., bacteria or fungi, in their natural environment, which are critical for clinical diagnosis or food safety purposes. To demonstrate this ability, we performed SRS spectroscopic imaging of a human blood sample mixed with living fungal cells *Candida albicans* (*C. albicans*), a species of *Candida* genus that can cause the candidiasis infection in humans. At 2940 cm^{-1}, all cells exhibited SRS signals with comparable signal intensities (Fig. 3(a)). However, in the spectral domain *C. albicans* cell bodies exhibited a strong Raman signal at 2940 cm^{-1} contributed by the CH_3 vibrations from protein, while, on the other hand, the lipid droplets showed an intense signal at a 2850 cm^{-1} peak from CH_2 vibrations. Meanwhile, blood cells, which were mostly dominated by red blood cells, showed broadband spectral profiles due to transient absorption signals from hemoglobin [26] (see Visualization 1). MCR analysis further decomposed the spectral features and distinguished *C. albicans* from red blood cells [Figs. 3(b) and 3(c)]. Another common infection cause of skin and respiratory infections, as well as food poisoning, *Staphylococcus aureus* (*S. aureus*), can also be separated from human red blood cells in the spectral window of 2800–3000 cm^{-1} [Figs. 3(d)–3(f)].

To demonstrate our speed advantage to a conventional SRS microscope that uses a motorized translational stage for delay-line tuning, as reported in Ref. [21], we imaged live *C. albicans* in blood using the latter system. At each Raman shift, an image composed of 400 × 400 pixels with a pixel dwell time of 1 μs was acquired, and the total acquisition time for 60 frames was ~30 s. Since the blood cells and *C. albicans* can move freely in solution, the location and orientation of every cell changed within one spectroscopic image stack (see Visualization 2). This sample movement severely perturbed the spectroscopic measurement and resulted in false spectral features (see Supplement 1, Fig. S5).

Finally, we show that our imaging platform can quantify the fat storage in three dimensions in a live *C. elegans*. *C. elegans* is an intact multicellular animal that is extensively used for studying the impact of lipid metabolism on aging and disease. Single-color CRS imaging using the C–H vibrational region has been demonstrated to visualize lipid storage [27,28], but the quantification remains difficult because most compartments exhibit a Raman signal in the C–H region. SRS spectroscopic imaging has been

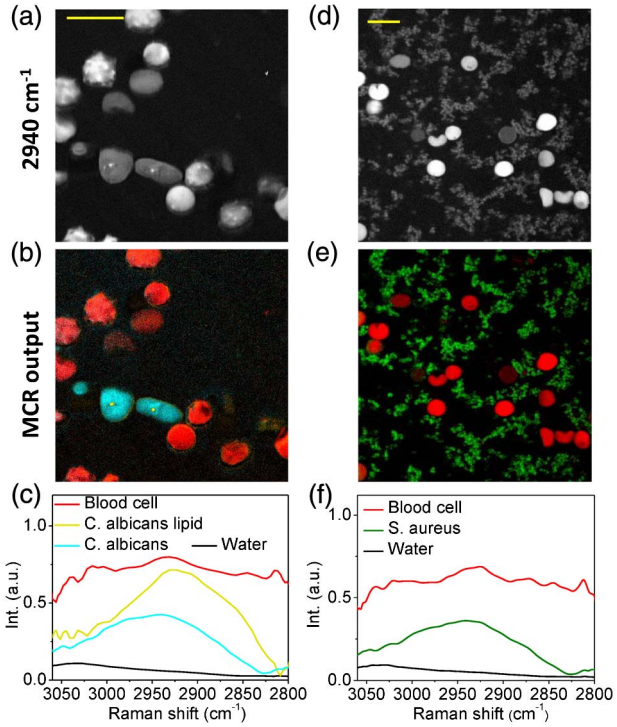

Fig. 3. SRS spectroscopic images of blood cells mixed with fungi/bacteria. (a) Raw SRS image of blood cells mixed with *C. albicans* at 2940 cm^{-1}. (b) MCR output concentration map of (a). (c) MCR output spectral profiles of (b). (d) Raw SRS image of blood cells mixed with *S. aureus* at 2940 cm^{-1}. (e) MCR output concentration map of (d). (f) MCR output spectral profiles of (e). Scale bar: 16 μm.

applied to identify and quantify lipid compartments at a cross-section of *C. elegans* based on the Raman region from 1620 to 1800 cm^{-1}, where the ratio of acyl C=C bond at 1655 cm^{-1} to ester C=O bond at 1745 cm^{-1} was used to identify different compartments [29]. In this study, fat stores were found to exhibit higher ratio of C=O to C=C than lysosome-related organelles (LROs), while protein showed a very weak signal at the C=O band. In addition, oxidized lipid droplets exhibited a shoulder at 1680 cm^{-1} in the region of the C=C band. However, *C. elegans* usually has a body that is several tens of micrometers thick, so 3-D chemical mapping of the lipid compartments is necessary to quantify fat storage.

Our new platform allowed 4-D SRS imaging (x–y–z–λ) of *C. elegans* in the fingerprint region. To demonstrate that the acyl C=C bond at 1655 cm^{-1} and ester C=O bond at 1745 cm^{-1} can be resolved by our system, we tuned the spectral window to 1600–1800 cm^{-1} and acquired an SRS spectrum from olive oil. Two peaks at 1655 and 1745 cm^{-1} were distinguished and matched with spontaneous Raman spectroscopy (see Supplement 1, Fig. S6). We then performed 4-D SRS images (x – y – z – λ) of an anesthetized *C. elegans* in the same spectral window. Each image, composed of 170 × 1700 pixels, was collected within 25 s, and 14 depth-resolved images were acquired with a 2 μm step size tuned manually by the microscope stage. Visualization 3 showed the spectroscopic image stack at a depth of 14 μm from the surface, and Visualization 4 presents a 3-D image stack at 1675 cm^{-1}. The 4-D image stack was then denoised and decomposed by MCR analysis. Figure 4(a) shows the

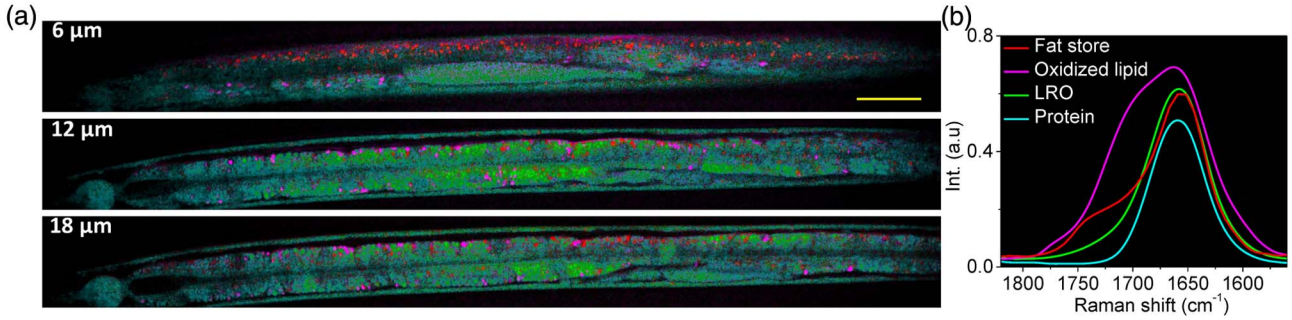

Fig. 4. SRS spectroscopic images of *C. elegans* at 6, 12, and 18 μm depths from the surface. (a) MCR output concentration maps at depths of 6, 12, and 18 μm from the surface. (b) MCR output spectra. Scale bar: 30 μm.

depth-resolved chemical maps of fat storage, LRO, oxidized lipid droplets, and protein, with their corresponding MCR spectral outputs shown in Fig. 4(b) and Visualization 5. The fat stores exhibited Raman peaks at 1655 and 1745 cm^{-1}. The LROs showed a peak at 1655 cm^{-1} and a weaker signal at 1745 cm^{-1}. The oxidized lipid droplets exhibited signals in the C═C and C═O regions together with a shoulder around 1700 cm^{-1}. Finally, the proteins showed a Raman peak at 1655 cm^{-1}. These results are in good agreement with our previous report in Ref. [29]. We further reconstructed the 3-D visualization of the *C. elegans* (Supplement 1, Fig. S7) in which the fat storage in intestinal cells over the entire worm body is clearly resolved.

In conclusion, we demonstrated real-time SRS spectroscopic imaging based on microsecond delay-line tuning. The SRS spectrum at each pixel was acquired within 83 μs, covering the 200 cm^{-1} spectral window with 25 cm^{-1} spectral resolution. The speed advantage allows chemical imaging of highly dynamic systems. Identification of pathogenic microorganisms, including bacteria and fungi, in blood samples was demonstrated. Our imaging platform also enabled 3-D chemical mapping of fat storage in live *C. elegans*. Collectively, the presented platform enables the use of Raman spectroscopy for early detection of microorganisms and compositional mapping of intracellular compartments in a living organism.

Funding. W. M. Keck Foundation; National Institutes of Health (NIH) (CA182608, GM114853).

Acknowledgment. JXC has a financial interest in Vibonix Inc.

See Supplement 1 for supporting content.

REFERENCES

1. A. Zumbusch, G. R. Holtom, and X. S. Xie, Phys. Rev. Lett. **82**, 4142 (1999).
2. C. W. Freudiger, W. Min, B. G. Saar, S. Lu, G. R. Holtom, C. He, J. C. Tsai, J. X. Kang, and X. S. Xie, Science **322**, 1857 (2008).
3. C. H. Camp and M. T. Cicerone, Nat. Photonics **9**, 295 (2015).
4. J. X. Cheng and X. S. Xie, Science **350**, aaa8870 (2015).
5. C. L. Evans, E. O. Potma, M. Puoris'haag, D. Côté, C. P. Lin, and X. S. Xie, Proc. Natl. Acad. Sci. USA **102**, 16807 (2005).
6. B. G. Saar, C. W. Freudiger, J. Reichman, C. M. Stanley, G. R. Holtom, and X. S. Xie, Science **330**, 1368 (2010).
7. C. Y. Lin, J. L. Suhalim, C. L. Nien, M. D. Miljkovic, M. Diem, J. V. Jester, and E. O. Potma, J. Biomed. Opt. **16**, 021104 (2011).
8. E. T. Garbacik, J. L. Herek, C. Otto, and H. L. Offerhaus, J. Raman Spectrosc. **43**, 651 (2012).
9. Y. Ozeki, W. Umemura, Y. Otsuka, S. Satoh, H. Hashimoto, K. Sumimura, N. Nishizawa, K. Fukui, and K. Itoh, Nat. Photonics **6**, 845 (2012).
10. D. L. Zhang, P. Wang, M. N. Slipchenko, D. Ben-Amotz, A. M. Weiner, and J. X. Cheng, Anal. Chem. **85**, 98 (2013).
11. F. Masia, A. Glen, P. Stephens, P. Borri, and W. Langbein, Anal. Chem. **85**, 10820 (2013).
12. M. Müller and J. M. Schins, J. Phys. Chem. B **106**, 3715 (2002).
13. J. X. Chen, A. Volkmer, L. D. Book, and X. S. Xie, J. Phys. Chem. B **106**, 8493 (2002).
14. C. H. Camp, Y. J. Lee, J. M. Heddleston, C. M. Hartshorn, A. R. H. Walker, J. N. Rich, J. D. Lathia, and M. T. Cicerone, Nat. Photonics **8**, 627 (2014).
15. C.-S. Liao, M. N. Slipchenko, P. Wang, J. Li, S.-Y. Lee, R. A. Oglesbee, and J.-X. Cheng, Light Sci. Appl. **4**, e265 (2015).
16. K. Seto, Y. Okuda, E. Tokunaga, and T. Kobayashi, Rev. Sci. Instrum. **84**, 083705 (2013).
17. C.-S. Liao, P. Wang, P. Wang, J. Li, H. J. Lee, G. Eakins, and J.-X. Cheng, Sci. Adv. **1**, e1500738 (2015).
18. D. Fu, F. K. Lu, X. Zhang, C. Freudiger, D. R. Pernik, G. Holtom, and X. S. Xie, J. Am. Chem. Soc. **134**, 3623 (2012).
19. T. Hellerer, A. M. K. Enejder, and A. Zumbusch, Appl. Phys. Lett. **85**, 25 (2004).
20. D. Fu, G. Holtom, C. Freudiger, X. Zhang, and X. S. Xie, J. Phys. Chem. B **117**, 4634 (2013).
21. B. Liu, H. J. Lee, D. L. Zhang, C.-S. Liao, N. Ji, Y. Q. Xia, and J.-X. Cheng, Appl. Phys. Lett. **106**, 173704 (2015).
22. X. M. Liu, M. J. Cobb, and X. D. Li, Opt. Lett. **29**, 80 (2004).
23. K. Hashimoto, M. Takahashi, T. Ideguchi, and K. Goda, Sci. Rep. **6**, 21036 (2016).
24. M. N. Slipchenko, R. A. Oglesbee, D. L. Zhang, W. Wu, and J.-X. Cheng, J. Biophoton. **5**, 801 (2012).
25. C.-S. Liao, J. H. Choi, D. Zhang, S. H. Chan, and J.-X. Cheng, J. Phys. Chem. C **119**, 19397 (2015).
26. D. L. Zhang, M. N. Slipchenko, D. E. Leaird, A. M. Weiner, and J.-X. Cheng, Opt. Express **21**, 13864 (2013).
27. M. C. Wang, W. Min, C. W. Freudiger, G. Ruvkun, and X. S. Xie, Nat. Methods **8**, 135 (2011).
28. M. Klapper, M. Ehmke, D. Palgunow, M. Bohme, C. Matthaus, G. Bergner, B. Dietzek, J. Popp, and F. Doring, J. Lipid Res. **52**, 1281 (2011).
29. P. Wang, B. Liu, D. L. Zhang, M. Y. Belew, H. A. Tissenbaum, and J.-X. Cheng, Angew. Chem. **53**, 11787 (2014).

128.46.89.36 {ts '2016-11-30 10:47:01'}